The influence of a Hamiltonian vibration versus a bath vibration on the 2D electronic spectra of a homodimer.

Ben S. Humphries,[1] Dale Green,[1] and Garth A. Jones[1,a)]
School of Chemistry, University of East Anglia, Norwich Research Park, Norwich, NR4 7TJ, UK

We elucidate the influence of system-bath boundary placement within an open quantum system (OQS), with emphasis on the 2DES spectral impacts, through application of the hierarchical equations of motion (HEOM) formalism for an exciton system. We apply two different models, the Hamiltonian vibration model (HVM) and bath vibration model (BVM), to a monomer and a homodimer. In the HVM we specifically include the vibronic states in the Hamiltonian capturing vibronic quenching, whereas in the BVM all vibrational detail is contained within the bath and described by an underdamped spectral density. The resultant spectra are analysed in terms of energetic peak position and thermodynamic broadening precision in order to evaluate the efficacy of the two models. The HVM produces 2D spectra with accurate peak positional information, whilst the BVM is well suited to modelling dynamic peak broadening. For the monomer, both models produce equivalent spectra in the limit where additional damping associated with the underdamped vibration in the BVM approaches zero. This is supported by analytical results. Whereas, for the homodimer, the BVM spectra are redshifted with respect to the HVM due to an absence of vibronic quenching in the BVM. The computational efficiency of the two models is also discussed in order to inform on the most appropriate use of each method.

Keywords: non-Markovian, HEOM, underdamped spectral density, 2D spectroscopy, homodimer

I. INTRODUCTION

Open quantum system (OQS) methodologies treat a quantum system of interest within the noisy environment in which it is embedded. Accurately modelling the dynamics of the quantum system requires not only good theoretical descriptions of both the system and the environment but also depends on the definition of the system-environment boundary. OQS approaches have been used to study a number of important processes in chemical physics such as electronic energy transfer (EET),[1–3] charge transfer,[4] as well as to investigate a number of phenomena of fundamental interest, for example, coherence.[5–8]

Experimentally, many processes occurring in molecular systems on the ultrafast timescale are investigated using time-resolved two-dimensional optical spectroscopy[9,10] which allows one to separate homogeneous and inhomogeneous spectral broadening as well as resolve electronic and vibronic couplings between quantum states. When it comes to accurately reproducing experimental two dimensional spectra using theoretical methodologies, it is imperative to correctly include any non-Markovian effects within the OQS dynamics. Non-Markovian effects are often interpreted as the quantum system having a memory of the state of the bath, but an alternative definition is in terms of the direction of the flow of information between the system and the bath.[11] The unidirectional flow of information from the system to the bath gives rise to Markovian dynamics while any flow of information from the bath back into the system results in non-Markovian behaviour. Accounting correctly for this non-Markovian behaviour in quantum trajectories is required for producing an accurate description of spectral broadening. In our previous work we quantitatively linked spectral broadening to the non-Markovian BLP (Breuer Laine Piilo) measure.[12]

Underdamped vibrational modes are defined as those that are coupled strongly to the electronic degrees of freedom of a molecular system, giving rise to oscillatory beating of exciton state energies, which results in slow dephasing of the reduced density matrix of the system of interest. This type of system is associated with strong non-Markovian behaviour, in which information returns back to the system from the bath. There are many ways to incorporate an underdamped vibration into an OQS, and it is not always immediately obvious which is best approach for a particular application, because there are a number of theoretical and computational implications that depend on your choice.[13] Most obviously, the underdamped vibration could be incorporated into the OQS in at least two ways; (1) as part of the quantum system itself, being defined explicitly in the system Hamiltonian or (2) as part of the environment via the spectral density that defines the bath. There are trade-offs when using either definition. In the former case, the additional vibronic structure requires a larger Hilbert space in order to explicitly define the additional vibronic coupling terms (even a single vibration will generally have multiple vibrational levels that need to be incorporated). On the other hand, in the latter case the Hilbert space of the system Hamiltonian is truncated but the spectral density will be more complex than that of a typical overdamped bath, resulting in a more mathematically detailed definition of the bath, resulting in more complicated OQS dynamics. As we show in this work, the two different ap-

a)Electronic mail: garth.jones@uea.ac.uk

proaches inevitably lead to different population dynamics and consequently different two-dimensional electronic spectra. One of the objectives of this paper is to understand the emergence of different features in the spectra when using different system-bath boundaries.

The nature of the dynamics for a particular OQS can be directly related to two key bath parameters: Δ which is the magnitude of the vibrations, and τ_c which is the correlation time of the bath. The product of the two, $\Delta \cdot \tau_c$, is a key parameter for *overdamped* systems. In the case of $\Delta \cdot \tau_c >> 1$ we observe inhomogeneous spectral broadening where slower bath fluctuations give rise to a particular instance of the OQS experiencing a different local environment. That is to say, the bath is moving slowly with respect to the timescale of the measurement.[10] On the other hand, in the case of the homogeneous limit, where $\Delta \cdot \tau_c << 1$ fast bath fluctuations mean that there is no correlation between measurements taken at different times, which results in different systems (or different instances of the same system) seeing the same noisy environment.[14]

The spectral density is particularly sensitive when the OQS is in neither the long nor short time limits, leading to spectral features that are neither purely Gaussian or purely Lorentzian. In order to model these cases non-Markovianity must be included in the dynamics. While it is still a matter of debate whether non-Markovianity favours coherent dynamics, there are a number of examples of coherent spectral phenomena being suppressed or enhanced by non-Markovianity within a system. Papers by Wu et al.,[15] Zhu et al.,[16] and Thoss et al.,[17] suggest that the Markovian approximation results in too much quantum coherence by neglecting memory effects in the dissipative bath. Specifically it is concluded by Wu et al.[15] through the use of the trace distance, that a robust control of quantum coherence is achieved by having an additional degree of freedom subsumed within the bath. In contrast Jing[18] presents a three-level quantum system coupled to a bosonic bath where Markovianity is shown to enhance coherent effects. It is clear that coherence is fundamental to atomic scale quantum phenomena, such as entanglement, and this in turn is affected by non-Markovian system dynamics. It is the coupling between a chaotic ensemble (the bath) and the quantum system of interest which interrupts the delicate balance required for coherence, resulting in decoherence.

A number of recent studies consider the impact of coherence on system dynamics, many from the perspective of aiming to reduce decoherence for physical applications, such as in Josephson junctions devices, but only a few studies consider the impact of where to place a vibrational mode within their model OQS. Huang and Zheng[19] theoretically study a qubit-oscillator system embedded in a noisy environment which acts as a tunable degree of freedom. These considerations were inspired by models which control the dissipative dynamics of a quantum-oscillator spin-boson system using a tunneling degree of freedom[20] and coherent behaviour influenced by strong coupling to a single bosonic mode.[21] In contrast, work by the authors Vierheilig,[22] Yao,[23] Ma,[24] and Man[25] consider an indirectly coupled qubit-bath system, or an effective qubit-bath system transformation of a qubit-nonlinear quantum oscillator-ohmic bath system. These works highlight the current interest in direct and indirect coupling to a noise bath, however, the focus of these studies was not whether an additional underdamped vibrational component within the bath would effect the system dynamics.

Following on from this, it is known that structured spectral densities have a profound impact on OQS dynamics[26] indicating that system-bath boundary considerations have practical as well as theoretical consequences that need to be considered. The work of Fujihashi et al.[27] consider quantum mechanical mixing among vibronic transitions in a weakly coupled heterodimer. In their work a spectral density is created for one of the two pigment molecules with a sharp vibrational peak, centred at approximately 200 cm^{-1}, induced by environmental fluctuations. This explores the impact on EET dynamics and 2D electronic spectra of environmental induced vibrational components within exciton states, but does not consider simpler systems. Chin and coworkers[7] consider overdamped and underdamped limits by studying the impact of different spectral densities, ranging from a Gaussian profile through to a Lorentzian and then a combination of both, on the decay of the correlation function for the HEOM. Their application is on vibrationally assisted energy transfer whereby they consider the collective mode signatures for each choice of spectral density and relate them to the non-Markovianity through the volume of accessible states in a Bloch sphere. Kim and coworkers[28] examine EET with a three-site Frenkel exciton model, with specific focus on the description of underdamped modes. Dynamics were compared where the underdamped mode was considered as either, part of the quantum subsystem, or as part of the classical bath, and they concluded that the classical approach produced equivalent results. Schröter et al.,[29] study dissipative exciton dynamics of a molecular heterodimer coupled to a Brownian oscillator bath through models produced using the HEOM. Linear absorption spectra are examined along with coherent oscillations in the population dynamics using Fourier spectrum analysis which reveals the origin of peaks in both the diabatic and adiabatic regimes by comparison with direct diagonalisation of a vibronic Hamiltonian. Importantly, they conclude by stating that further research into 2DES would be required in order to link these conclusions directly to experimental spectra; which is the focus of this paper.

Historically a number of perturbative approaches have been employed to model OQS for EET in vibronic systems. The quantum system of interest is kept deliberately distinct from the stochastic bath degrees of freedom, and is modelled explicitly in order to retain as much accuracy as possible but with maximum computational efficiency. In turn, the stochastic bath is typi-

cally described by a continuous spectral density function rather than a (infinite) system of individual harmonic oscillators. Notable examples of perturbative methods include: the Redfield equation, Förster rate theory, generalized quantum master equations, and Langevin equation approaches.[30–36] However in this work we use the well known non-perturbative approach,[37] the hierarchical equations of motion (HEOM), originally developed by Tanimura et al.[38–44] which is one of the most successful and commonly employed in recent years. It models the memory effects of the interaction of the quantum system of interest through evolution of an hierarchy of auxiliary density operators (ADOs). In particular this method has been applied to the study of electron transfer[16,45–50], exciton dynamics,[27,29,51–54] and excited state dynamics within the condensed phase.[55]

The accuracy of the HEOM when applied to molecular systems is what makes it particularly suitable for testing the hypothesis of this paper,[44] which is focused on definition of the OQS boundary. Specifically, we consider a vibronic homodimer system capable of transferring an exciton coherently between its chromophores. The chromophore vibration is strongly coupled to the exciton states, and can be included in one of two ways: either (1) using an overdamped bath to represent the environment, in combination with the intramolecular vibration explicitly defined within the Hamiltonian (we refer to as the *Hamiltonian vibration* model, HVM), or (2) using underdamped dynamics in which the effects of the intramolecular vibration are introduced into the bath through the spectral density (we refer to as the *bath vibration* model, BVM). The question we address is whether subsuming the intramolecular vibration into the bath is equivalent to defining it in the Hamiltonian; in particular with reference to the resulting two-dimensional spectra. Phenomenologically these two approaches appear to be qualitatively the same, as they should result in similar fluctuations of the exciton states, however, the size of the Hilbert space for the quantum system is greatly reduced in case (2). This leads to a clear practical motivation to this study, namely the trade-off between accuracy of the results compared to the computational cost of the dynamics. The HVM requires a larger Hilbert space but the BVM has a significantly more complex spectral density and therefore more auxiliary density matrices need to be simultaneously evolved within the HEOM formalism.

In this paper, we describe a series of time-resolved two-dimensional electronic spectra (2D spectra)[56–58] for model monomer and dimer chromophore systems. In both cases, the electronic (excitonic) states are strongly coupled to an intramolecular vibrational mode. We investigate the short-time evolution of the 2D spectra for each of the systems, when described by the Hamiltonian vibration model, and the bath vibration model. As outlined in the discussion of results, there are a number of differing features within the spectra that reflect different approximations of the model. One must therefore carefully consider the form of the system-bath model when using OQS dynamics to interpret 2D spectra.

II. METHODOLOGY

A. Construction of the system Hamiltonian

The homodimer system is formed by the electronic coupling of a pair of identical monomers which are modelled with harmonic potentials for each of the ground and singly excited states, $|g\rangle$ and $|e\rangle$, representing an intramolecular vibrational mode. As such the monomer Hamiltonian is,

$$\mathrm{H}_M = |g\rangle\, h_g\, \langle g| + |e\rangle\, h_e\, \langle e|\,, \tag{1}$$

where the nuclear Hamiltonians for the ground and excited electronic states are,

$$h_g = \hbar\omega_0 \left(b^\dagger b + \frac{1}{2}\right), \tag{2}$$

$$h_e = \hbar\left(\omega_{eg}^0 + \lambda\right) + \hbar\omega_0 \left(b^\dagger b + \frac{1}{2} - \frac{\Delta_0}{\sqrt{2}}(b + b^\dagger)\right). \tag{3}$$

Here ω_{eg}^0 is the frequency of the transition between the ground and excited electronic states, and ω_0 is the vibrational mode frequency. The excited state potential is displaced with respect to the ground state minimum along the dimensionless nuclear coordinate by Δ_0, resulting in the reorganisation energy, $\hbar\lambda = \frac{1}{2}\hbar\omega_0\Delta_0^2$. Applying the Born-Oppenheimer approximation, the monomer (M) basis states are the tensor product of the electronic and nuclear degrees of freedom,

$$|\psi_M\rangle = |\alpha_M\rangle \otimes |\nu_M\rangle = |\alpha_M, \nu_M\rangle\,, \tag{4}$$

where $\alpha = g, e$ and $\nu = 0, 1, 2, \ldots$ such that the off-diagonal terms, proportional to $(b + b^\dagger)$ where $b^{(\dagger)}$ is the lowering (raising) operator,[59] account for vibronic coupling with the displaced excited state. Transitions between the ground and excited electronic states are then mediated by the transition dipole moment $\boldsymbol{\mu}_M$.

Construction of the homodimer (D) then starts by combining the monomer Hilbert spaces. A composite Hilbert space is defined based on the states of both constituent monomers, where $M = 1, 2$ for each monomer,

$$|\psi_D\rangle = |\alpha_1, \nu_1\rangle \otimes |\alpha_2, \nu_2\rangle = |\alpha_1, \nu_1, \alpha_2, \nu_2\rangle\,. \tag{5}$$

The monomers are treated as collinear point dipoles which are also collinear with the displacement vector,

$$\mathbf{R} = R\hat{\mathbf{R}}, \tag{6}$$

and are coupled via the Förster equation,

$$J = \frac{\boldsymbol{\mu}_1 \cdot \boldsymbol{\mu}_2 - 3(\boldsymbol{\mu}_1 \cdot \hat{\mathbf{R}})(\boldsymbol{\mu}_2 \cdot \hat{\mathbf{R}})}{4\pi\epsilon_r\epsilon_0 R^3}. \tag{7}$$

The total dimer Hamiltonian[60–62] is then,

$$\begin{aligned}\mathrm{H}_D =& \mathrm{H}_1 \otimes \mathrm{I}_2 + \mathrm{I}_1 \otimes \mathrm{H}_2 \\ &+ J \sum_{\nu_1,\nu_2} \left(|e_1,\nu_1,g_2,\nu_2\rangle\langle g_1,\nu_1,e_2,\nu_2| \right. \\ &+ \left. |g_1,\nu_1,e_2,\nu_2\rangle\langle e_1,\nu_1,g_2,\nu_2|\right), \end{aligned} \tag{8}$$

where I_M is the identity matrix over the degrees of freedom of the M^{th} monomer, such that the coupling represents transfer of electronic excitation only, with vibrational quanta unchanged.[59,63]

The eigenstates of the dimer Hamiltonian, $|\phi_D\rangle$, correspond to the delocalized exciton states and give the diagonalised dimer Hamiltonian,

$$\mathrm{H}'_D = \mathrm{U}^\dagger \mathrm{H}_D \mathrm{U}, \tag{9}$$

where $\mathrm{U} = \sum_k |\phi_{D,k}\rangle\langle\psi_{D,k}|$. The simulations discussed below use the diagonalised Hamiltonian for both the monomer and homodimer.

The collinear arrangement of transition dipole moments creates a J-aggregate[64,65] which has a common ground state, $|g\rangle$, a lower energy, bright exciton state corresponding to the symmetric combination of singly excited states, $|e^+\rangle$, a higher energy, dark exciton state corresponding to the anti-symmetric combination of singly excited states, $|e^-\rangle$, and a doubly excited state, $|f\rangle$, corresponding to the simultaneous excitation of both monomers (ignoring the biexciton binding energy).[26,62,66] An energy level diagram[67] showing the allowed/forbidden transitions of the homodimer for the HVM and BVM models is shown in figure 1.

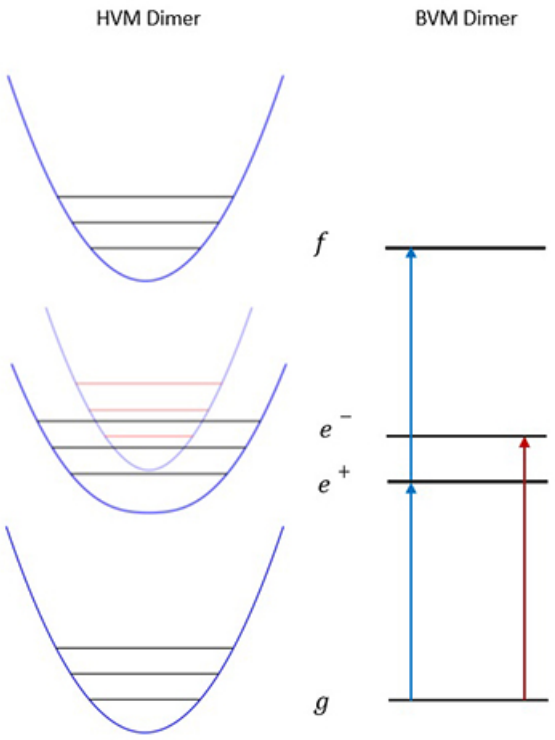

FIG. 1: Energy level diagrams for the HVM and BVM dimers. The bright (e^+) and dark (e^-) exciton potentials are both plotted along the antisymmetric vibrational coordinate.[68] Blue and red arrows correspond to allowed and forbidden electronic transitions, respectively.

B. The two open system models

The homodimer system is then coupled to its environment, which is modelled as an open quantum system. We compare two different models which define the intramolecular vibration either within the system Hamiltonian (HVM) or the bath spectral density (BVM), corresponding to movement of the system-bath boundary; figure 2. Both approaches use HEOM methods, and the full details of this are presented in our previous paper.[12]

The HEOM method derived by Tanimura and coworkers[38,39] models the environment as a bath of harmonic oscillators which represent phonon modes. The spectral density consists of a continuum of bath modes with masses, m_α, frequencies, ω_α, and distribution of coupling strengths, g_α such that the spectral density is defined as,

$$J(\omega) = \sum_\alpha \frac{g_\alpha^2}{2m_\alpha\omega_\alpha}\delta(\omega-\omega_\alpha). \tag{10}$$

In accordance with the fluctuation-dissipation theorem, the entirety of the environment degrees of freedom, including non-Markovian effects, are then described by the system-bath correlation function,

$$C(t) = \frac{\hbar}{\pi}\int_0^\infty J(\omega)\left(\coth\left(\frac{\beta\hbar\omega}{2}\right)\cos(\omega t) - i\sin(\omega t)\right)\mathrm{d}\omega, \tag{11}$$

where $\beta = (k_\mathrm{B}T)^{-1}$. The imaginary term within the integrand of this contour integral corresponds to dissipative effects within the bath whilst the real term corresponds to the thermally induced fluctuations within the system. HEOM methods are then derived from an approximated analytical form of the spectral density, as discussed in our previous paper, ref. 12.

In the HVM, the full vibronic monomer and homodimer Hamiltonians from the previous section are coupled to the Debye spectral density,[69]

$$J_o(\omega) = \frac{2\eta_o\omega\Lambda_o}{\omega^2+\Lambda_o^2}, \tag{12}$$

representing intermolecular solvent modes and are propagated using the overdamped (o) HEOM described in ref. 12. $J_o(\omega)$ is shown in figure 3, dominated by lower frequency modes, with a peak at Λ_o with intensity η_o. $\Lambda_o = \tau_c^{-1}$ defines the rate of decay of system-bath correlations and is chosen to be slow enough such that there is

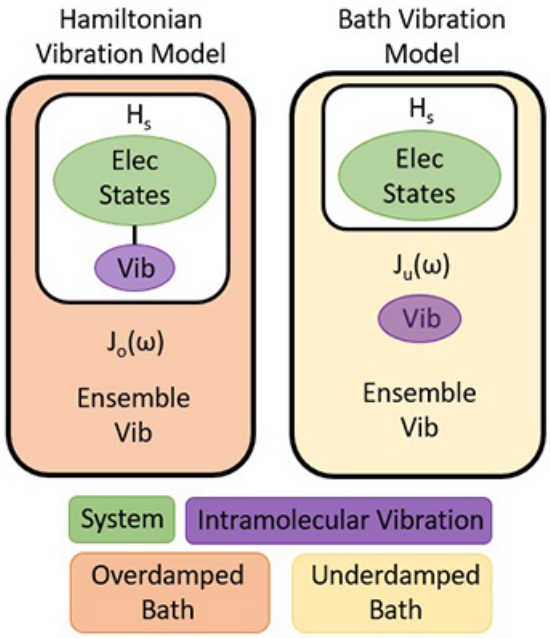

FIG. 2: Diagrammatic description of the Hamiltonian and bath vibration models.

visible inhomogeneous broadening in the resulting spectra.

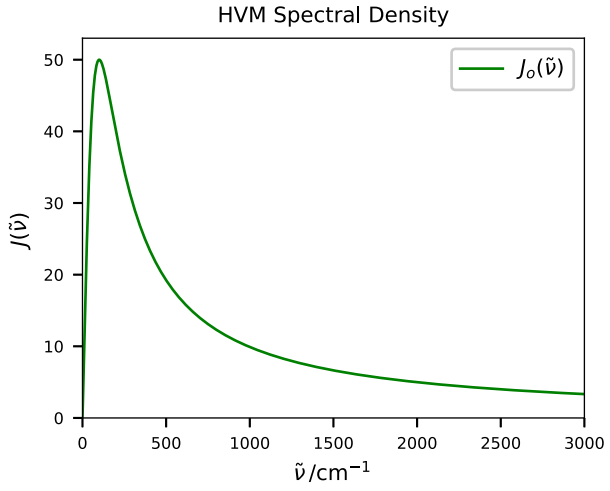

FIG. 3: Overdamped spectral density for the HVM.

The bath couples to the electronic excited states through the operators,

$$\mathrm{V}_M = \sum_{\nu_M} |e_M, \nu_M\rangle\langle e_M, \nu_M| \,, \tag{13}$$

for the monomer and,

$$\begin{aligned}\mathrm{V}_D = \sum_{\nu_1,\nu_2} \big(& |e_1,\nu_1,g_2,\nu_2\rangle\langle e_1,\nu_1,g_2,\nu_2| \\ & + |g_1,\nu_1,e_2,\nu_2\rangle\langle g_1,\nu_1,e_2,\nu_2| \\ & + 2\,|e_1,\nu_1,e_2,\nu_2\rangle\langle e_1,\nu_1,e_2,\nu_2| \big),\end{aligned} \tag{14}$$

for the dimer, which undergo the same unitary transformation as the diagonalisation of the Hamiltonian; $\mathrm{V}' = \mathrm{U}^\dagger \mathrm{V} \mathrm{U}$. The stochastic motion of the bath thus causes the electronic transition frequencies to fluctuate leading to dephasing of excited state wavepackets and spectral broadening. Vibrational relaxation and dephasing can be included by coupling the intramolecular mode coordinate to a second bath with a separate spectral density,[61,70,71] and recent studies have also highlighted the impact of fluctuations in the electronic coupling strength to EET, accounting for the nuclear dependence of the electronic transition dipole moment, beyond the Condon approximation.[55,72,73] But here, the HVM is simplified to account for an undamped vibrational mode with constant J, assuming vibrational relaxation and any fluctuations in the electronic coupling are much slower processes than electronic dephasing, with negligible effect on the 2DES spectra at very early population times, $T \leq 100$ fs.

In the BVM, the intramolecular vibrational mode is subsumed into the bath degrees of freedom through a canonical transformation. This reduces the size of the system Hamiltonian to the electronic states only, which are then coupled to an underdamped (u) Brownian oscillator which adds to the spectral density.

The spectral density for the BVM has two components,[74]

$$J_u(\omega) = \frac{2\eta_1\gamma_1\omega_1^2\omega}{(\omega_1^2-\omega^2)^2+\gamma_1^2\omega^2} + \frac{2\eta_2\gamma_2\omega_2^2\omega}{(\omega_2^2-\omega^2)^2+\gamma_2^2\omega^2}, \tag{15}$$

where the first corresponds to the intramolecular vibrational mode in the underdamped limit,[69] $\omega_1 \gg \gamma_1$, such that $\omega_1 = \omega_0$ and $\eta_1 = \lambda$ from eq. 3, and the second represents the bath modes from the HVM model. In the overdamped limit, where $\omega_2 \ll \gamma_2$ this reduces to the Debye form,

$$J_u(\omega) = \frac{2\eta_1\gamma_1\omega_1^2\omega}{(\omega_1^2-\omega^2)^2+\gamma_1^2\omega^2} + \frac{2\eta_2\omega\Lambda}{\omega^2+\Lambda^2}, \tag{16}$$

where,

$$\Lambda = \frac{\omega_2^2}{\gamma_2}. \tag{17}$$

The total spectral density for the BVM is shown in figure 4 as well as the separate underdamped, $J_1(\omega)$, and overdamped, $J_2(\omega)$, components. In contrast to the broad overdamped spectral density for the low frequency bath modes, the underdamped spectral density features

a sharp Lorentzian peak at the intramolecular mode frequency with width determined by the damping parameter γ_1.

For the BVM, an underdamped HEOM described in ref. 12 is derived from eq. 15, corresponding to two underdamped baths. Both baths couple to the electronic excited states through the dephasing operators,

$$\mathrm{V}'_M = |e\rangle\langle e|\,, \tag{18}$$

for the monomer and,

$$\mathrm{V}'_D = |e^+\rangle\langle e^+| + |e^-\rangle\langle e^-| + 2\,|f\rangle\langle f|\,, \tag{19}$$

for the dimer. Note that γ_1 introduces additional damping of the intramolecular mode in the BVM, absent in the HVM. Approaching the limit $\gamma_1 \to 0$, the BVM becomes equivalent to the undamped intramolecular vibrational mode in the HVM. But zero damping invalidates the HEOM termination criterion,[12] producing an infinite hierarchy, and thus some minimal damping is unavoidable.

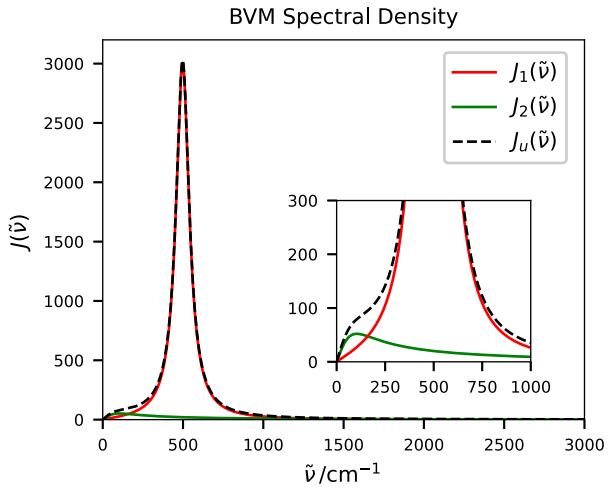

FIG. 4: Underdamped spectral density for the BVM.

Figure 1 then highlights the difference between the definition of the system in the HVM vs. BVM, building upon figure 2. In the HVM, the system Hamiltonian defines the vibrational levels for each electronic state, fully accounting for vibronic coupling terms, whereas the BVM contains the electronic states only. In both models, the system Hamiltonians are renormalised as $\mathrm{H}' + \sum_i \eta_i (\mathrm{V}'_i)^2$, where i are the components of the spectral density, to counter the energy shift induced by the system-bath coupling.[44,75]

2D electronic spectra[66,71,76,77] are calculated in the impulsive limit using the response function formalism, as described in the appendix of ref. 12, using the HEOM to correctly account for non-Markovian system-bath interactions across system-field interactions.

In the following simulations, the ground and excited electronic states of the monomer are separated by $\tilde{\omega}^0_{eg} = 10\,000\,\mathrm{cm}^{-1}$ where tilde denotes conversion to wavenumbers, $\tilde{\omega}^0_{eg} = \omega^0_{eg}(2\pi c)^{-1}$. The electronic states are coupled to a vibrational mode with $\tilde{\omega}_0 = 500\,\mathrm{cm}^{-1}$, with the excited state displaced by $\Delta_0 = 1.09$ such that $\lambda = 300\,\mathrm{cm}^{-1}$. The monomer transition dipole moments are then strongly coupled by $\tilde{J} = -400\,\mathrm{cm}^{-1}$ forming the J-aggregate homodimer. After diagonalisation, the monomer and homodimer Hamiltonians are truncated to the $\nu_M = 0, 1, 2$ vibrational levels only.

For the HVM overdamped bath, $\tilde{\eta}_o = 50\,\mathrm{cm}^{-1}$ with $\tilde{\Lambda}_o = 100\,\mathrm{cm}^{-1}$ such that $\Delta\tau_c = 1.44$. For the BVM underdamped baths, $\eta_1 = \lambda$, $\omega_1 = \omega_0$, $\tilde{\gamma}_1 = 100\,\mathrm{cm}^{-1}$, $\eta_2 = \eta_o$, $\tilde{\omega}_2 = 500\,\mathrm{cm}^{-1}$ and $\tilde{\gamma}_2 = 2500\,\mathrm{cm}^{-1}$ such that $\Lambda = \Lambda_o$. At 300 K with the Markovian limit set to be $2000\,\mathrm{cm}^{-1}$, HVM and BVM propagates 50 and 26091 ADOs, respectively. 2D spectra are calculated with coherence time up to $\tau = 200$ fs in steps of 0.5 fs, for population times of $T = 0, 50$ and 100 fs.

III. RESULTS AND DISCUSSION

The monomer spectra. The calculated time-resolved spectra allow comparison between the BVM and HVM and for determining the efficacy of the two methods. Figures 5 and 6, as shown below, depict the monomer spectra obtained using the two models. Our expectation is a strong agreement between the two models barring the unavoidable additional damping in the BVM. Figures 5 and 6 present distinct peaks at the fundamental frequency, ω^0_{eg}, in agreement with the theory in addition to peaks due to vibronic pathways at plus and minus integer multiples of the mode frequency, ω_0. These peaks are particularly distinct in the HVM due to the explicit construction of the Hamiltonian with three vibrational levels, per electronic state, resulting in a Hilbert space $|\alpha\rangle \otimes |\nu\rangle$ of $\dim(\mathcal{H}) = 6$. The BVM has a Hilbert space $\dim(\mathcal{H}) = 2$ because it accounts for the electronic states only to produce a two level system. Clear evidence of vibronic cross peaks shows that the system vibration is manifested in both the HVM and BVM despite the different ways in which the vibrational mode is incorporated into the models. Furthermore, oscillation of vibrational coherence pathways[56] over the waiting time, T, results in peak amplitude changes within both spectra in figures 5 and 6. The similarity between these peak intensities suggests that both models are able to capture all the essential features for the monomer.

However, there are also some noteworthy differences based on the complementary setup of the models. At $T = 0$ fs in the HVM, figure 5, there is uniform elongation of vibronic peaks along the diagonal which is lost as the waiting time increases. In contrast, peaks within the BVM are smooth and poorly defined with significant overlap between neighbouring peaks, and increased broadening below the diagonal reflects the additional vibronic peaks as the BVM is not limited to three vibrational levels, as is the case for the HVM. Spectral dif-

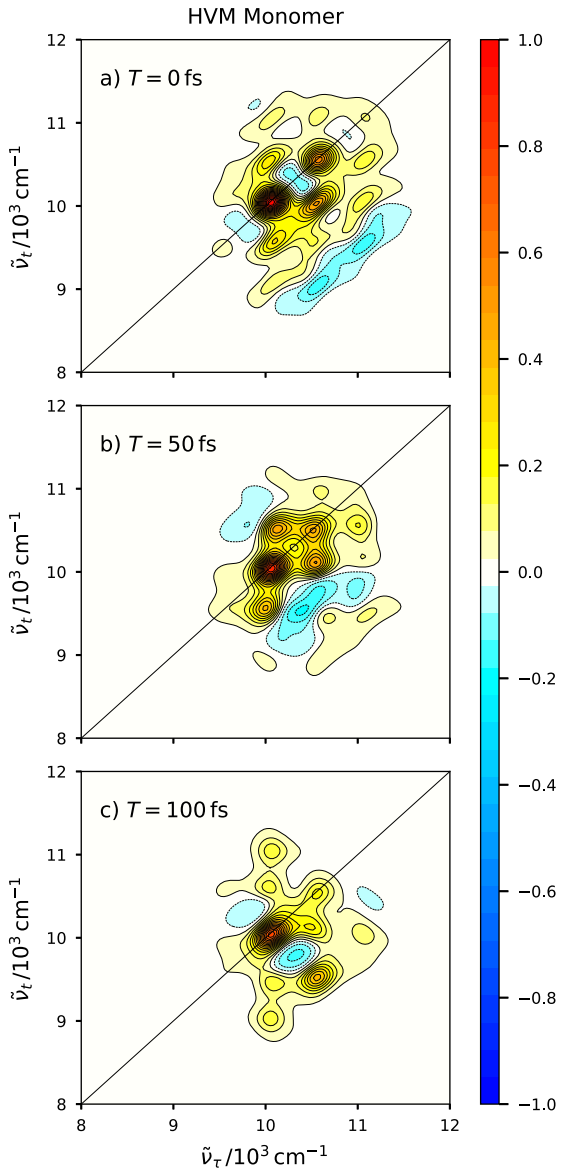

FIG. 5: Absorptive 2D spectra for the HVM monomer at $T = 0, 50$ and 100 fs, normalised to the maximum at $T = 0$ fs.

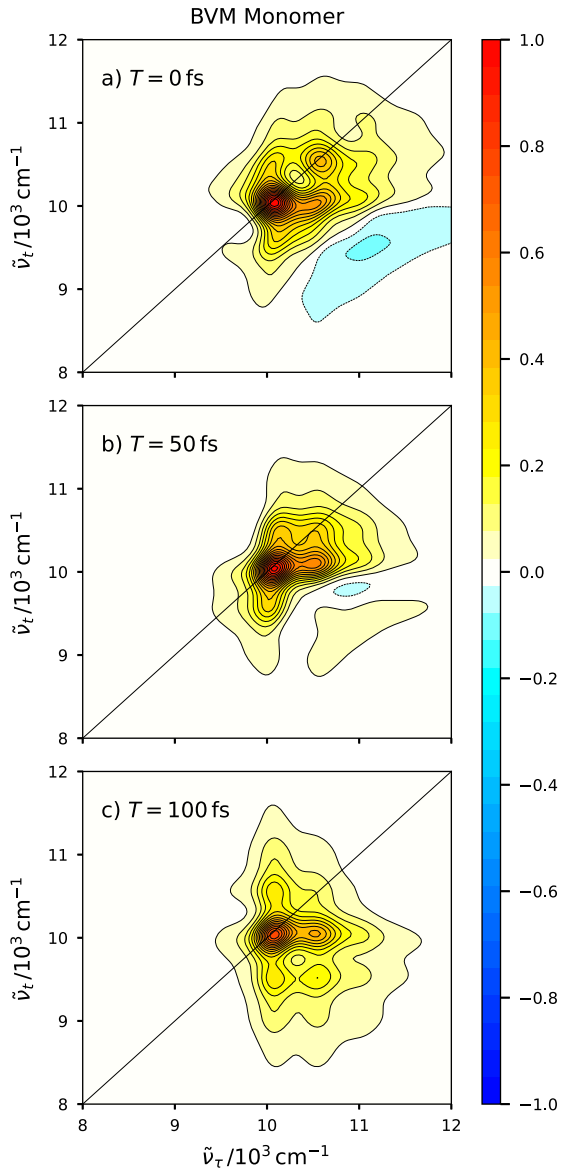

FIG. 6: Absorptive 2D spectra for the BVM monomer at $T = 0, 50$ and 100 fs, normalised to the maximum at $T = 0$ fs.

fusion is clearly observed in the HVM, in contrast to the BVM spectra, where diffusion is obscured by the greater broadening which is a consequence of the additional damping intrinsic to the underdamped mode.

Finally we note that both spectra in figures 5 and 6 have significant regions of negative intensity below the diagonal at $T = 0$ fs. These are the result of rephasing vibrational coherence pathways which oscillate with opposite phase above and below the diagonal[69,78] and should not be mistaken for excited state absorption peaks, which are not observed for a monomer with only two electronic states.

The dimer spectra. Next we consider the strongly coupled dimer. In agreement with the analysis for the monomer we observe similarities in the peak positions and the peak intensities for both the HVM and BVM. We expect a redshift of J of the fundamental peak from ω_{eg}^0 to $\omega_{e^+g}^0$ corresponding to the formation of a J-aggregate. In both figures 7 and 8 the theoretically predicted fundamental peak and peaks resulting from additions of the fundamental transition with integer multiples of the mode frequency[79] are clearly present. In addition to these peaks we also observe strong excited state absorption peaks above the diagonal, corresponding to transitions from the $|e^+\rangle$ to $|f\rangle$ doubly excited state. The next similarity between the HVM and BVM dimer

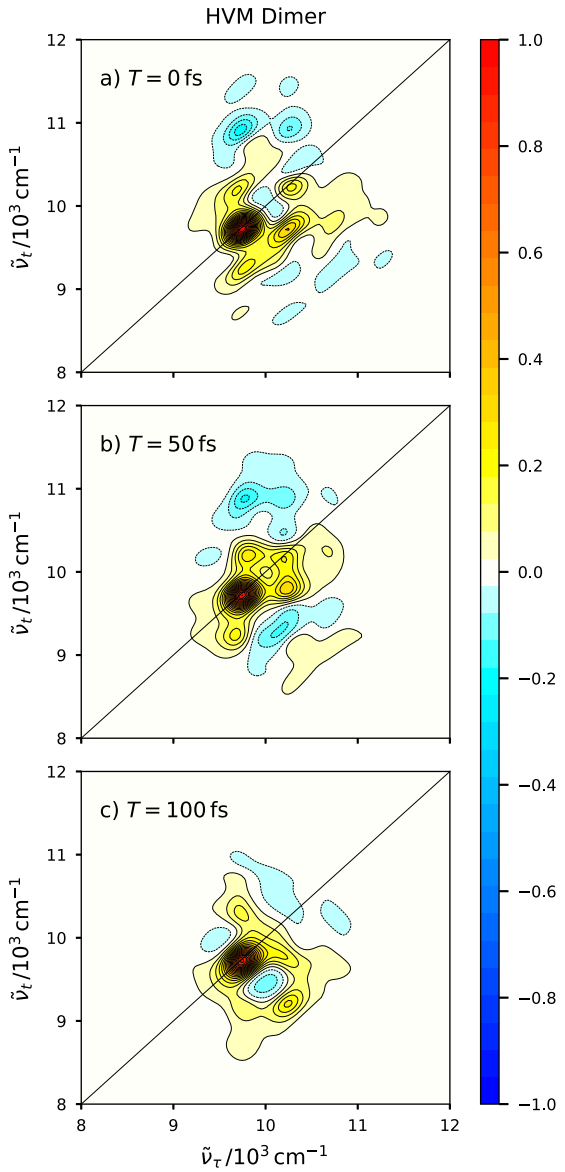

FIG. 7: Absorptive 2D spectra for the HVM dimer at $T = 0, 50$ and $100\,\mathrm{fs}$, normalised to the maximum at $T = 0\,\mathrm{fs}$.

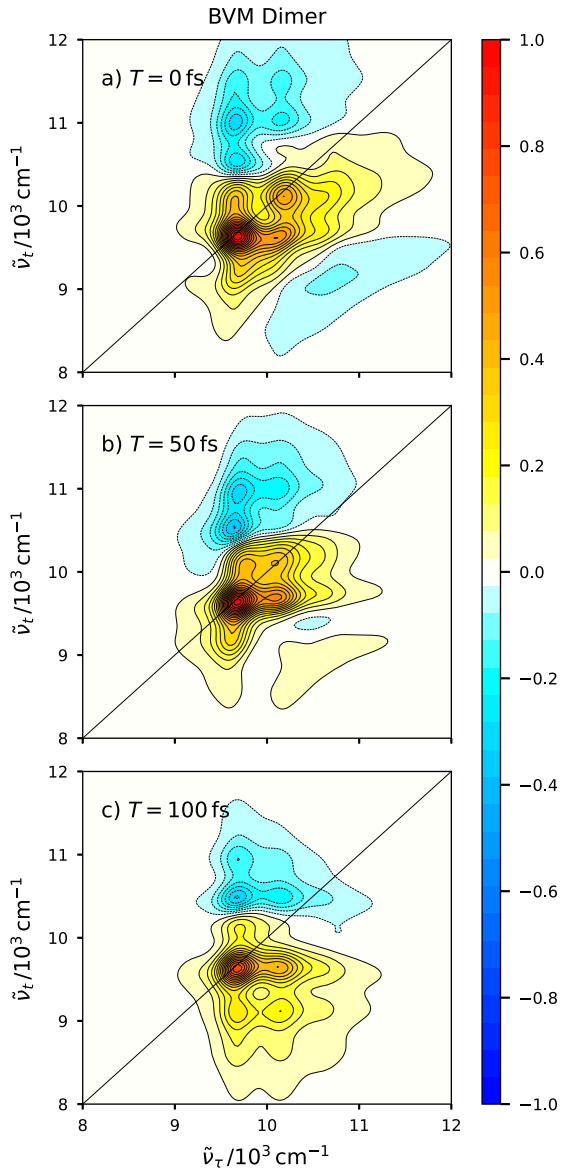

FIG. 8: Absorptive 2D spectra for the BVM dimer at $T = 0, 50$ and $100\,\mathrm{fs}$, normalised to the maximum at $T = 0\,\mathrm{fs}$.

spectra is the increased amplitude of the fundamental peak relative to that of the vibronic peaks in both the HVM and BVM.[80] Additionally the spectra present comparable peak amplitudes with increasing waiting time, T, due to the oscillation of the vibrational coherence pathways.[81] These key similarities highlight the presence of vibronic pathways, even involving the extended excited state structure of the dimer, for both the HVM and BVM.

In contrast to these similarities we note a number of key differences between the spectra produced using the two models. In agreement with the monomer results, there is a uniform broadening along the diagonal in the HVM which is absent in the BVM. This highlights that the impact on the broadening due to direct coupling of the vibrational states to overdamped environment modes is not dependent on the system choice. The other important difference is related to redshifting of the entire spectra. Our expectation based on the theory for J-aggregates is that there will be a redshift of $\tilde{J} = -400\,\mathrm{cm}^{-1}$ which is quenched[68,82,83] by the vibronic coupling of the system to a reduced magnitude. This quenched dimer redshift is directly observable in the HVM spectra in figure 7 and matches the decrease in transition frequency relative to the monomer shown by the Hamiltonian eigenvalues for the system of

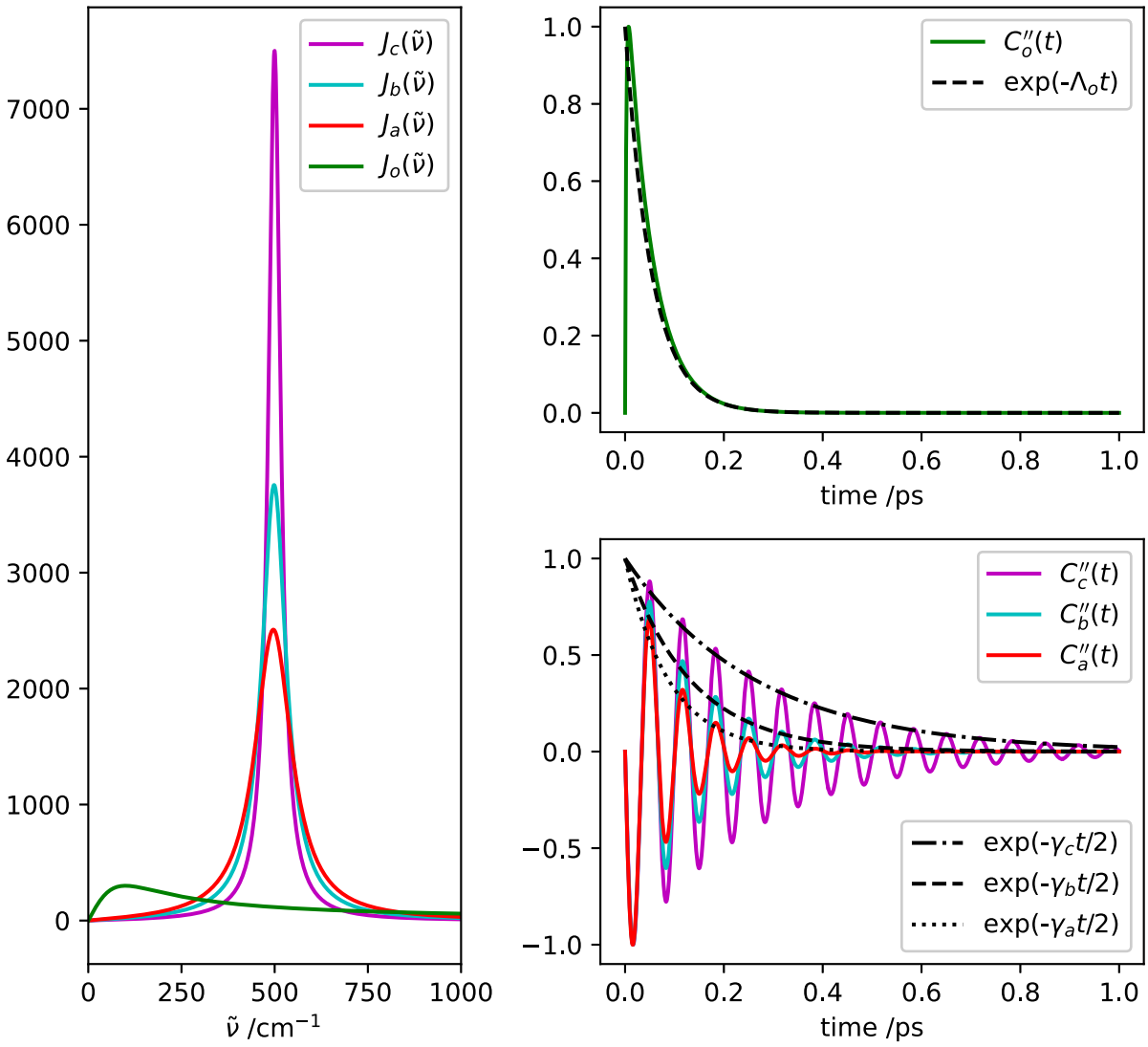

FIG. 9: Spectral densities and correlation functions, with exponential fits, for an overdamped, $\tilde{\Lambda}_o = 100$, and three underdamped spectral densities with damping strengths $\tilde{\gamma}_a = 120$ cm^{-1}, $\tilde{\gamma}_b = 80$ cm^{-1}, and $\tilde{\gamma}_c = 40$ cm^{-1}.

$-316\,\mathrm{cm}^{-1}$. However there is a striking difference in redshift between the two models. In the BVM, both the eigenvalues and spectra in figure 8 show a full redshift of $\tilde{J} = -400$ cm^{-1} with a complete absence of vibronic quenching. This demonstrates an important intrinsic difference between the two models: vibronic quenching is absent in BVM dimer systems.

Comparison of broadening between HVM and BVM. One of the fundamental differences presented by comparison of the BVM and HVM in these models is the significantly different broadening each method presents. In order to correctly attribute these differences in spectral lineshape to the placement of the fundamental vibration we consider a series of spectra with decreasing damping strengths, $\tilde{\gamma}_a = 120$ cm^{-1}, $\tilde{\gamma}_b = 80$ cm^{-1}, and $\tilde{\gamma}_c = 40$ cm^{-1}, for the BVM approaching the limit of $\tilde{\gamma}_1 \to 0$. Initially we consider the HVM, where all of the vibrational information is contained within the Hamiltonian, coupled to a single overdamped spectral density. This spectral density is of Ohmic form with a high frequency cutoff and is applied in order to introduce electronic dephasing to the system through the interaction with bath modes. In the BVM the intramolecular mode of interest is moved from the Hamiltonian and introduced into the spectral density. An undamped mode has no decaying component and subsequently introduces no additional dephasing time to the total system and does not add to the overall broadening of the 2DES. However, due to the nature of the HEOM, and because the spectral density is required to have a representation in exponen-

tial form, the introduction of some level of damping is unavoidable.

In order to demonstrate the influence of the additional damping from the underdamped spectral density the correlation function from equation (11) is formally solved, when $J_1(\tilde{\nu})$ is substituted for $J(\omega)$, and expanded into real and imaginary parts.[84]

$$C(t) = C'(t) + iC''(t), \tag{20}$$

In the overdamped regime, with a single spectral density, the correlation function reduces to an exponential decay, $\exp(-t/\tau_c)$. Figure 9 shows the spectral density for the HVM, its calculated correlation function, and the exponential decay.

In all three of the underdamped regimes the correlation function is not just a simple decay. When the correlation function both decays and oscillates we expect the decay to have a rate of $\tilde{\gamma}_x/2$, where x denotes the damping strength. This follows from the simplification of the imaginary part of the correlation function:[84]

$$C''(t) = \frac{\hbar\eta\omega_0^2}{2\zeta}\sin(\zeta t)\exp\left(-\frac{\tilde{\gamma}_x}{2}|t|\right), \tag{21}$$

where $\zeta = \sqrt{\omega_0^2 - (\tilde{\gamma}_x/2)^2}$.

Figure 9 shows the correlation functions and negative exponential dephasing rates calculated using $\tilde{\gamma}_x$, for all three underdamped spectral densities. As demonstrated in figure 9, decreasing the damping increases the dephasing time, approaching the limit of an undamped vibration corresponding to a continuous oscillation in the correlation function.

Figure 10 shows the application of these spectral densities to the BVM for the monomer. The successive reduction of γ shows a clear trend towards the lineshape of the HVM (Figure 5a), however there are computational implications to this. The number of ADOs increases exponentially as a function of the reduction of damping strength such that for a $\tilde{\gamma}$ reduction of 40 cm^{-1} (such as between $\tilde{\gamma}_b$ and $\tilde{\gamma}_c$) an additional 115,620 ADOs are required. Consequently it is not computationally tractable to perform simulations with very small damping strengths. Furthermore, the termination procedure implemented in this HEOM cannot be applied to undamped modes, where $\gamma = 0$.

Subsuming the fundamental vibration of the dimer into the spectral density has a considerable impact on the dynamics, as previously discussed, and this is due to the structure of the Hamiltonian used in the HEOM model. The HVM calculations for the dimer have three vibrational levels in the constituent monomer units leading to a Hilbert space $\dim(\mathcal{H}) = 36$ for the dimer, whereas the BVM assumes monomers are two level systems, resulting in a Hilbert space $\dim(\mathcal{H}) = 4$ for the dimer.[26] Consequently the HVM contains all relevant couplings between the energy levels giving rise to an equally large

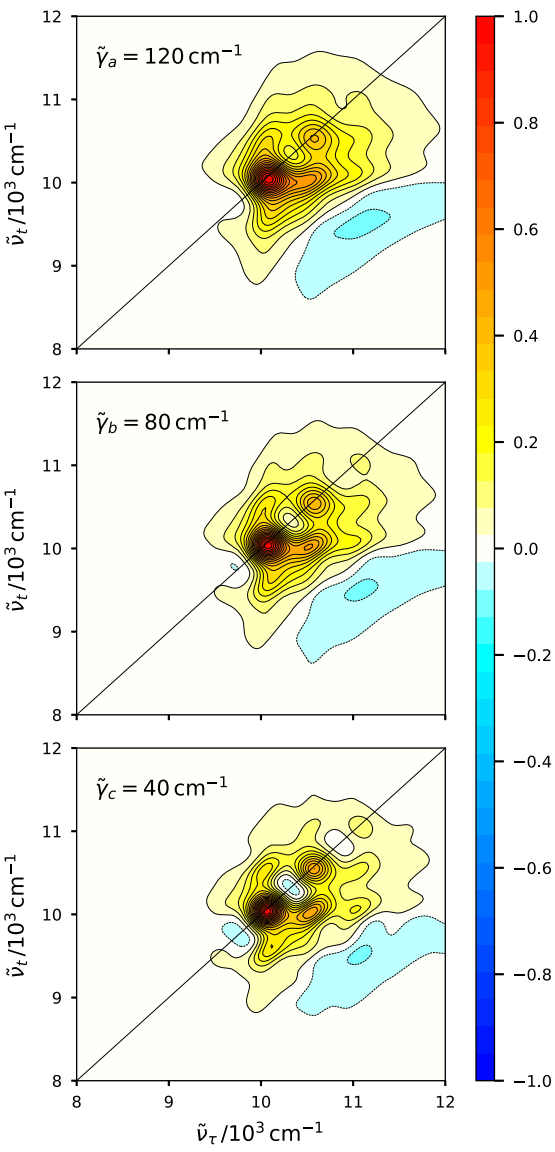

FIG. 10: Absorptive 2D spectra for the BVM monomer at $T = 0\,\text{fs}$, normalised to the maximum at $T = 0\,\text{fs}$, with damping strengths $\tilde{\gamma}_a = 120\ \text{cm}^{-1}$, $\tilde{\gamma}_b = 80\ \text{cm}^{-1}$, $\tilde{\gamma}_c = 40\ \text{cm}^{-1}$.

number of sharply defined peaks.[26] For the HVM, the peak information and energy transfer pathways in the dimer originate within the Hamiltonian, whereas in the BVM they occur as the result of non-Markovian feedback from energy fluctuations within the bath. Additionally in the HVM, the broadening applied to each peak is a uniform broadening due to the overdamped environment modes. Overall this results in more Lorentzian-shaped peaks that present more precise positional information.

In contrast, because the BVM has a relatively smaller Hamiltonian, the vibronic peaks and broadening are calculated based on an underdamped spectral density which is a combination of both the bath modes and the sub-

sumed vibration. Subsequently the additional damping leads to more pronounced broadening of each peak and this broadening is not uniform, that is to say differing peaks have different lineshapes. As such the BVM spectra have fewer explicit off-diagonal peaks, where vibronic peaks arise naturally through the broadening introduced by the spectral density.

This has implications for the computational costs of the two different models. The truncation of the Hilbert space by removal of explicit vibronic states in the BVM reduces the computational cost of the diagonalisation when compared to the HVM. However, the increased computational cost of the BVM comes from the spectral density, and resulting HEOM, which is required in order to describe an underdamped vibration.

IV. CONCLUSIONS

This research focuses on elucidating the impact of the placement of the system-bath boundary, how it affects OQS dynamics, and subsequent differences in 2DES spectra. To this end, we applied two different models, the HVM and BVM, to a monomer and a homodimer. In the HVM we specifically include the vibronic states in the Hamiltonian capturing vibronic quenching, whereas in the BVM all vibrational detail is contained within the bath and described by an underdamped spectral density. The analysis for the resulting models focuses on the comparison between the HVM and BVM approaches with specific emphasis on the impact on 2DES spectra.

The model for the monomer successfully reproduces expected spectral features for both models, but there are some differences in the broadening. Due to the construction of the BVM, the uniform broadening applied to each peak from the Hamiltonian is obscured as a consequence of the unavoidable additional damping from the underdamped mode. Figures 9 and 10 show a successive reduction in the damping strength during which the BVM spectra converge towards that of the HVM. It can be seen that in the limit of $\gamma_1 \to 0$ the two models become equivalent.

Results for the dimer also present all expected features for both models and differences in spectral broadening consistent with that of the monomer have been observed. However, the choice of the system-bath boundary placement clearly alters the vibronic coupling effects, as is evidenced by the lack of vibronic quenching relative to the Hamiltonian eigenvalues for the BVM. It is clear from these results that HVM versus BVM is a choice between energetic informational precision (peak position) and greater dynamic broadening, respectively. This represents a shift in focus from an accurate system Hamiltonian to a model that efficiently includes a more complete system-bath interaction.

In addition to these conclusions, we also present observations about the relative computational effort for each model. In the HVM we specifically include the vibronic states in the Hamiltonian, capturing vibronic quenching, but it is expensive because of the diagonalisation: the computational bottleneck is the system choice and the corresponding Hilbert space dimension. In contrast, the BVM contains all vibrational detail within the bath as an underdamped spectral density allowing the Hilbert space dimension to be significantly reduced. Application of the BVM shifts the computational bottleneck to the bath dynamics, exponentially increasing the number of ADOs as a function of decreasing damping strength. However, this introduces the risk of neglected vibronic quenching and additional damping which results in greater peak broadening across the spectrum.

ACKNOWLEDGMENTS

The research presented in this paper was carried out on the High Performance Computing Cluster supported by the Research and Specialist Computing Support service at the University of East Anglia. B.S.H thanks the Faculty of Science, University of East Anglia for studentship funding. G.A.J. and D.G. acknowledge support from the Engineering and Physical Sciences Research Council under Awards No. EP/V00817X/1.

CONFLICTS OF INTEREST

The authors have no conflicts of interest to disclose.

DATA AVAILABILITY

The data that support the findings of this contribution are available from the corresponding authors upon reasonable request.

V. REFERENCES

[1] Y. Yan, Y. Liu, T. Xing, and Q. Shi, WIREs Comput. Mol. Sci. **11**, 1 (2021).
[2] M.-J. Tao, N.-N. Zhang, P.-Y. Wen, F.-G. Deng, Q. Ai, and G.-L. Long, Sci. Bull. **65**, 318 (2020), 1907.06528.
[3] X. Leng, T. N. Do, P. Akhtar, H. L. Nguyen, P. H. Lambrev, and H. Tan, Chem. – An Asian J. **15**, 1996 (2020).
[4] A. De Sio, X. T. Nguyen, and C. Lienau, Zeitschrift für Naturforsch. A **74**, 721 (2019).
[5] B. González-Soria, F. Delgado, and A. Anaya-Morales, J. Phys. Conf. Ser. **1730**, 012033 (2021), 2008.07580.
[6] V. Balevičius and C. D. P. Duffy, Photosynth. Res. **144**, 301 (2020).
[7] A. Chin, E. Mangaud, V. Chevet, O. Atabek, and M. Desouter-Lecomte, Chem. Phys. **525**, 110392 (2019).
[8] J. C. Dean and G. D. Scholes, Acc. Chem. Res. **50**, 2746 (2017).
[9] D. M. Jonas, Annu. Rev. Phys. Chem. **54**, 425 (2003).
[10] M. Khalil, N. Demirdöven, and A. Tokmakoff, J. Phys. Chem. A **107**, 5258 (2003).
[11] E.-M. Laine, J. Piilo, and H.-P. Breuer, EPL (Europhysics Lett. **92**, 60010 (2010), 1004.2184.

[12] D. Green, B. S. Humphries, A. G. Dijkstra, and G. A. Jones, J. Chem. Phys. **151**, 174112 (2019).
[13] V. A. Mikhailov and N. V. Troshkin, Phys. Rev. A **103**, 012208 (2021), 2005.12897.
[14] P. Hamm and M. Zanni, *Concepts and Methods of 2D Infrared Spectroscopy* (Cambridge University Press, Cambridge, 2011).
[15] W. Wu and H.-Q. Lin, Phys. Rev. A **94**, 062116 (2016), 1612.05338.
[16] L. Zhu, H. Liu, and Q. Shi, New J. Phys. **15**, 095020 (2013).
[17] M. Thoss, H. Wang, and W. H. Miller, J. Chem. Phys. **115**, 2991 (2001).
[18] J. Jing and T. Yu, Phys. Rev. Lett. **105**, 240403 (2010), 1009.5301.
[19] P. Huang and H. Zheng, Chem. Phys. Lett. **500**, 256 (2010), 0908.1454.
[20] Z. Lü and H. Zheng, J. Chem. Phys. **136**, 121103 (2012).
[21] E. K. Levi, E. K. Irish, and B. W. Lovett, Phys. Rev. A **93**, 042109 (2016), 1510.00608.
[22] C. Vierheilig, D. Bercioux, and M. Grifoni, Phys. Rev. A **83**, 012106 (2011), 1010.4684.
[23] Y. Yao, Phys. Rev. B **93**, 115426 (2016), 1510.06798.
[24] T. Ma, Y. Chen, T. Chen, S. R. Hedemann, and T. Yu, Phys. Rev. A **90**, 042108 (2014), 1404.5280.
[25] Z.-X. Man, N. B. An, and Y.-J. Xia, Opt. Express **23**, 5763 (2015).
[26] M. Schröter, S. Ivanov, J. Schulze, S. Polyutov, Y. Yan, T. Pullerits, and O. Kühn, Phys. Rep. **567**, 1 (2015).
[27] Y. Fujihashi, G. R. Fleming, and A. Ishizaki, J. Chem. Phys. **142**, 212403 (2015), 1505.05281.
[28] C. W. Kim, W.-G. Lee, I. Kim, and Y. M. Rhee, J. Phys. Chem. A **123**, 1186 (2019).
[29] M. Schröter, T. Pullerits, and O. Kühn, Ann. Phys. **527**, 536 (2015).
[30] M. F. Blackwell, J. Chem. Phys. **83**, 5589 (1985).
[31] M. T. Wong and Y.-C. Cheng, J. Chem. Phys. **154**, 154107 (2021).
[32] M. Bundgaard-Nielsen, J. Mørk, and E. V. Denning, Phys. Rev. B **103**, 235309 (2021), 2103.14327.
[33] W. T. Pollard and R. A. Friesner, J. Chem. Phys. **100**, 5054 (1994).
[34] R. Kubo, M. Toda, and N. Hashitsume, *Statistical Physics II Nonequilibrium Statistical Mechanics*, 2nd ed. (Springer-Verlag Berlin Heidelberg).
[35] T. Förster, Ann. Phys. **437**, 55 (1948).
[36] T. Renger, V. May, and O. Kühn, Phys. Rep. **343**, 137 (2001).
[37] F. Levi, S. Mostarda, F. Rao, and F. Mintert, Reports Prog. Phys. **78**, 082001 (2015).
[38] Y. Tanimura and R. Kubo, J. Phys. Soc. Japan **58**, 101 (1989).
[39] Y. Tanimura, Phys. Rev. A **41**, 6676 (1990).
[40] Y. Tanimura and T. Steffen, J. Phys. Soc. Japan **69**, 4095 (2000).
[41] Y. Tanimura, J. Phys. Soc. Japan **75**, 082001 (2006).
[42] Y. Tanimura, J. Chem. Phys. **141**, 044114 (2014).
[43] Y. Tanimura, J. Chem. Phys. **142**, 144110 (2015), 1502.04077.
[44] Y. Tanimura, J. Chem. Phys. **153**, 020901 (2020).
[45] J. Strümpfer and K. Schulten, J. Chem. Phys. **131**, 225101 (2009).
[46] A. Ishizaki and G. R. Fleming, Proc. Natl. Acad. Sci. **106**, 17255 (2009).
[47] J. M. Moix, J. Ma, and J. Cao, J. Chem. Phys. **142**, 094108 (2015), 1501.05679.
[48] Q. Shi, L. Chen, G. Nan, R. Xu, and Y. Yan, J. Chem. Phys. **130**, 164518 (2009).
[49] M. Tanaka and Y. Tanimura, J. Chem. Phys. **132**, 214502 (2010).
[50] M. Tanaka and Y. Tanimura, J. Phys. Soc. Japan **78**, 073802 (2009).
[51] A. G. Dijkstra and V. I. Prokhorenko, J. Chem. Phys. **147**, 064102 (2017).
[52] J. Seibt and O. Kühn, J. Phys. Chem. A **125**, 7052 (2021).
[53] R. Dutta and B. Bagchi, J. Phys. Chem. A **125**, 4695 (2021).
[54] M. Cainelli and Y. Tanimura, J. Chem. Phys. **154**, 034107 (2021), 2101.08869.
[55] S. Ueno and Y. Tanimura, J. Chem. Theory Comput. **17**, 3618 (2021), 2102.02427.
[56] F. V. de A. Camargo, L. Grimmelsmann, H. L. Anderson, S. R. Meech, and I. A. Heisler, Phys. Rev. Lett. **118**, 033001 (2017).
[57] R. Borrego-Varillas, A. Nenov, L. Ganzer, A. Oriana, C. Manzoni, A. Tolomelli, I. Rivalta, S. Mukamel, M. Garavelli, and G. Cerullo, Chem. Sci. **10**, 9907 (2019).
[58] A. Gelzinis, R. Augulis, V. Butkus, B. Robert, and L. Valkunas, Biochim. Biophys. Acta - Bioenerg. **1860**, 271 (2019).
[59] V. Butkus, L. Valkunas, and D. Abramavicius, J. Chem. Phys. **140**, 034306 (2014), 1310.1343.
[60] A. Chenu, N. Christensson, H. F. Kauffmann, and T. Mančal, Sci. Rep. **3**, 2029 (2013), 1211.4397.
[61] H.-G. Duan, M. Thorwart, and R. J. D. Miller, J. Chem. Phys. **151**, 114115 (2019), 1904.04033.
[62] V. Butkus, D. Zigmantas, D. Abramavicius, and L. Valkunas, Chem. Phys. Lett. **587**, 93 (2013), 1305.2525.
[63] V. Tiwari, W. K. Peters, and D. M. Jonas, Proc. Natl. Acad. Sci. **110**, 1203 (2013).
[64] N. J. Hestand and F. C. Spano, Chem. Rev. **118**, 7069 (2018).
[65] N. S. Ginsberg, Y.-C. Cheng, and G. R. Fleming, Acc. Chem. Res. **42**, 1352 (2009).
[66] S. Polyutov, O. Kühn, and T. Pullerits, Chem. Phys. **394**, 21 (2012).
[67] A. Eisfeld, L. Braun, W. T. Strunz, J. S. Briggs, J. Beck, and V. Engel, J. Chem. Phys. **122**, 134103 (2005).
[68] S. Kopec, P. Ottiger, S. Leutwyler, and H. Köppel, J. Chem. Phys. **137**, 184312 (2012).
[69] V. Butkus, L. Valkunas, and D. Abramavicius, J. Chem. Phys. **137**, 044513 (2012), 1205.3383.
[70] D. I. G. Bennett, P. Malý, C. Kreisbeck, R. van Grondelle, and A. Aspuru-Guzik, J. Phys. Chem. Lett. **9**, 2665 (2018), 1803.06389.
[71] S.-H. Yeh, R. D. Hoehn, M. A. Allodi, G. S. Engel, and S. Kais, Proc. Natl. Acad. Sci. **116**, 18263 (2019).
[72] M. H. Lee and A. Troisi, J. Chem. Phys. **146** (2017), 10.1063/1.4976558.
[73] J. Seibt and T. Mančal, Chem. Phys. **515**, 129 (2018), arXiv:1807.07475.
[74] Y. Tanimura, J. Chem. Phys. **137**, 22A550 (2012).
[75] A. G. Dijkstra and Y. Tanimura, J. Chem. Phys. **142**, 212423 (2015), 1502.06410.
[76] A. Halpin, P. J. M. Johnson, R. Tempelaar, R. S. Murphy, J. Knoester, T. L. C. Jansen, and R. J. D. Miller, Nat. Chem. **6**, 196 (2014).
[77] H.-G. Duan, P. Nalbach, V. I. Prokhorenko, S. Mukamel, and M. Thorwart, New J. Phys. **17**, 072002 (2015).
[78] V. Butkus, D. Zigmantas, L. Valkunas, and D. Abramavicius, Chem. Phys. Lett. **545**, 40 (2012), 1201.2753.
[79] R. Tempelaar, A. Halpin, P. J. M. Johnson, J. Cai, R. S. Murphy, J. Knoester, R. J. D. Miller, and T. L. C. Jansen, J. Phys. Chem. A **120**, 3042 (2016).
[80] F. P. Diehl, C. Roos, A. Duymaz, B. Lunkenheimer, A. Köhn, and T. Basché, J. Phys. Chem. Lett. **5**, 262 (2014).
[81] E. Romero, V. I. Novoderezhkin, and R. van Grondelle, Nature **543**, 355 (2017).
[82] P. Ottiger, H. Köppel, and S. Leutwyler, Chem. Sci. **6**, 6059 (2015).
[83] P. Ottiger, S. Leutwyler, and H. Köppel, J. Chem. Phys. **136**, 174308 (2012).
[84] S. Mukamel, *Principles of Nonlinear Optical Spectroscopy*, edited by M. Lapp, J.-i. Nishizawa, B. B. Snavely, A. C. Tam, and T. Wilson (Oxford University Press, Oxford, 1995).